THE ASTROPHYSICAL JOURNAL, 372:67–80, 1991 May 1

THE MOLECULAR INTERSTELLAR MEDIUM AND THE NEAR-INFRARED CONTINUUM OF THE BARRED LINER NGC 6764

A. ECKART, M. CAMERON, J. M. JACKSON, R. GENZEL, AND A. I. HARRIS
Max-Planck-Institut für Physik und Astrophysik, Institut für Extraterrestrische Physik, 8046 Garching, Germany
W. WILD
European Southern Observatory, Karl-Schwarzschild-Strasse 2, 8046 Garching, Germany
AND
H. ZINNECKER
Institut für Astronomie und Astrophysik, Universität Würzburg, Am Hubland, 8700 Würzburg, Germany
Received 1990 July 30; accepted 1990 October 12

ABSTRACT

We report measurements of isotopic CO line emission and J, H, K near-infrared continuum emission of the barred spiral NGC 6764. The optical, near-infrared, and millimeter data are in excellent agreement with a brief and intense starburst at the nucleus. This finding is supported by the Wolf-Rayet emission-line features seen in the nucleus of the galaxy which are direct evidence for recent massive star formation. Toward the nucleus the molecular interstellar medium is moderately warm and dense. Simple, one-component model calculations of radiative transfer show that the minimum beam-averaged temperature of the gas is of the order of 20 K, and that the molecular hydrogen density ranges between 3×10^3 and 3×10^4 cm^{-3}. In the arms the molecular gas is either subthermally excited, and/or the kinetic temperature is less than 10 K. The ratio between far-infrared (FIR) luminosity and molecular hydrogen masses is in the range of values expected for noninteracting starburst galaxies. Comparing the morphologies of the near-infrared continuum and ^{12}CO line emission, we find that most of the molecular gas is associated with a massive, barlike, nuclear stellar bulge. The near-infrared colors of the spiral bar are in agreement with colors expected for late-type stars and Sc galaxies. Applying the beam-averaged molecular column density, we estimate an extinction of $A_V = 3$–4 mag toward the nucleus. The dereddened nuclear colors are indicative for a composite galactic nucleus resulting from significant contributions of both a power-law source and a stellar component.

By comparing NGC 6764 to a starburst galaxy, elliptical radio galaxy, Seyfert galaxy, and a quasar, we conclude that, judged from the two lowest rotational levels of CO, these sources show common beam-averaged properties of the molecular gas: the bulk of the nuclear molecular line emission arises in warm, dense, optically thick gas. The CO line emission in the disks and arms of the galaxies arises from cold and probably subthermally excited gas.

Subject headings: galaxies: individual (NGC 6764) — galaxies: interstellar matter — galaxies: nuclei — interstellar: molecules

1. INTRODUCTION

Recently a number of evolutionary models of the interstellar media of different classes of extragalactic sources have been suggested (e.g., Norman & Scoville 1988; Sanders et al. 1988; Rieke, Lebofsky, & Walker 1988). A key test of these evolutionary sequences is to investigate the variation of concentration and excitation of the molecular material in the nuclei of a sample of galaxies representing the different classes. In the course of such a systematic effort we present new measurements of the two lowest CO isotopic rotational transitions and the near-infrared continuum emission from the S-shaped, barred spiral galaxy NGC 6764 at a redshift of about 2420 km s^{-1} (Rubin, Thonnard, & Ford 1975). Because of the strong optical line emission of its nucleus, Rubin et al. (1975) classified it initially as a Seyfert 2 galaxy. Further studies by Osterbrock & Cohen (1982) revealed a low-excitation optical spectrum that classifies NGC 6764 as a LINER galaxy. The initial studies by Rubin et al. (1975) showed evidence for both tangential and radial motions in the nucleus. At the nucleus the galaxy exhibits a stellar optical continuum source with a "width" of about 1".6 (Rubin et al. 1975). Osterbrock & Cohen (1982) found the nucleus to exhibit the 466 nm Wolf-Rayet emission feature, which is only seen in a small number of galaxies (Armus, Heckman, & Miley 1988). This feature is taken as direct evidence for recent massive star formation in the nuclei of these objects.

Single-dish radio observations at 20 cm (Heckman, Balick, & Sullivan 1978) and 6 cm (Sramek 1975) show a radio spectrum with a spectral index of -1.0, indicative of synchrotron radiation (see flux densities listed in Table 5). Very Large Array (VLA) radio continuum maps at 6 cm wavelength have been published by Ulvestad, Wilson, & Sramek (1981) and Wilson & Willis (1980). They find a slightly resolved central component and diffuse emission extending about 10" to the southeast perpendicular to the bar. Observations of the 21 cm H I emission line have been reported by Shostak (1978) and Heckman et al. (1978). Both authors infer a total H I mass of $2 \times 10^9\ h^{-2}\ M_\odot$ ($h = H_0/100$ km s^{-1} Mpc^{-1}) and a ratio between the H I mass and the total mass of about 0.07, typical for spirals (Shostak 1978).

A first detection of the ^{12}CO(1–0) line toward NGC 6764 using the NRAO 12 m telescope has been reported by Sanders & Mirabel (1985). Here we present extensive new measurements of the $J = 1$–0 and $J = 2$–1 rotational transitions of

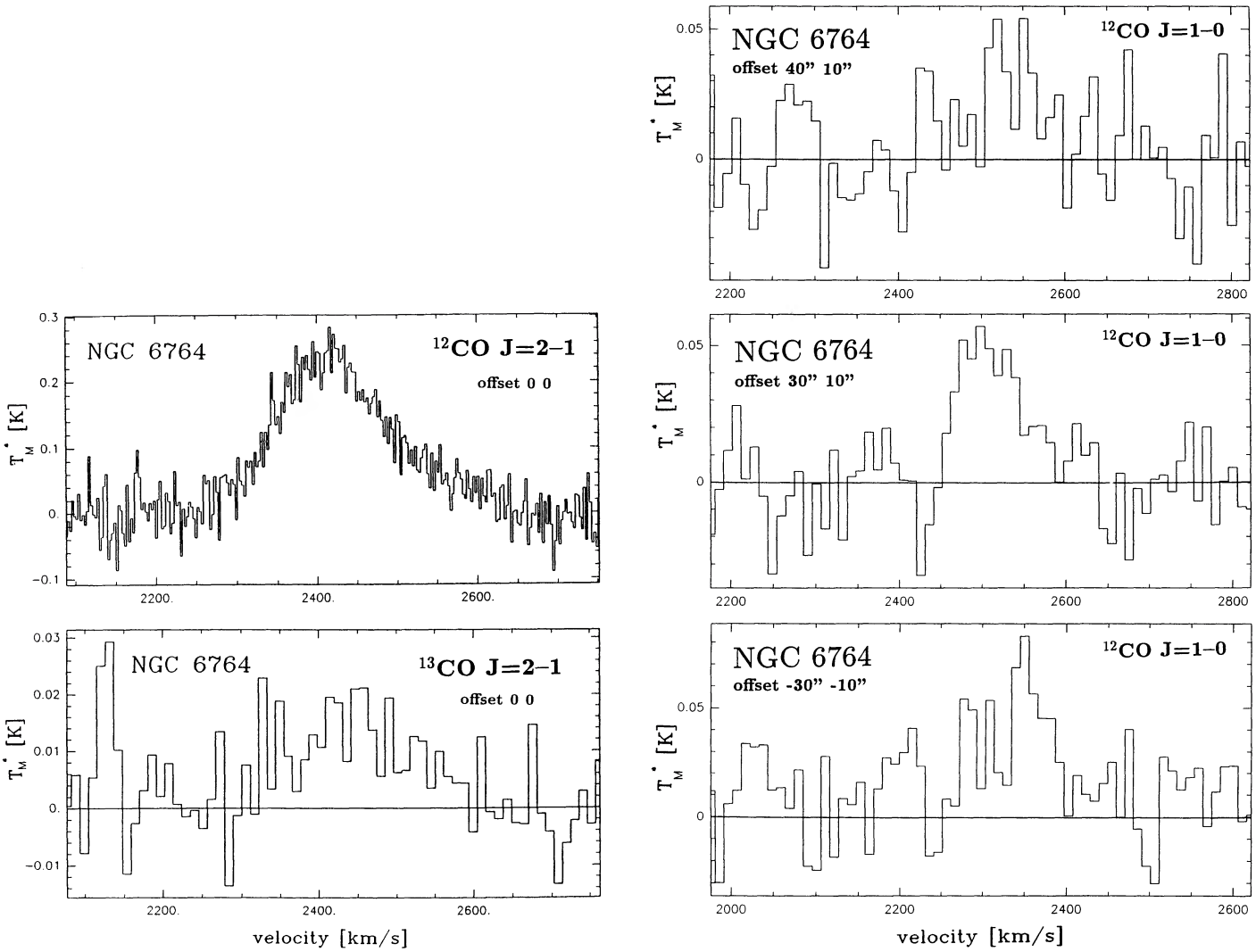

FIG. 1.—(*a*) ^{12}CO(2–1) and ^{13}CO(2–1) spectrum at the central position of NGC 6764. The spectral resolutions are 2.6 and 10.4 km s^{-1} per channel. The ^{12}CO(2–1) spectrum is a sum of all spectra taken at the central position and corresponds to a total integration time of 53 minutes. The ^{13}CO(2–1) spectrum results from a deep integration of 95 minutes. Both spectra were taken separately. (*b*) ^{12}CO(2–1) spectra about 40″ NE, 30″ NE, and 30″ SW of the nucleus on the bar of NGC 6764. The integration times are 50, 40, and 50 minutes, respectively. The spectral resolution is 10.4 km s^{-1} per channel.

^{12}CO and ^{13}CO obtained with the 30 m IRAM telescope and the first *J*, *H*, *K* images of this object obtained with the 3.8 m United Kingdom Infrared Telescope (UKIRT). The millimeter observations provide first information on the dynamics, spatial distribution, and physical state of the molecular interstellar gas.

2. OBSERVATIONS

2.1. *The Millimeter Observations*

The millimeter observations were carried out with the IRAM 30 m telescope in 1987 October, 1988 September, and 1990 February. We used the IRAM SIS receivers (Blundell et al. 1985; Blundell, Carter, & Gundlach 1988) and a filter bank of 512 × 1 MHz channels to observe the $J = 1$–0 and $J = 2$–1 rotational transitions of ^{12}CO and ^{13}CO in the nuclear region of NGC 6764. Figure 1*a* shows the ^{12}CO(2–1) and ^{13}CO(2–1) spectra at the central position. Figure 1*b* shows ^{12}CO(1–0) spectra off nucleus on the arms. Table 1 summarizes the system parameters at 115 GHz and 230 GHz. For observations at three positions in the bar of NGC 6764, the small line widths allowed us to split the filter bank into two 256 × 1 MHz channels and thus to observe simultaneously at 115 GHz and 230 GHz. The system was calibrated by the chopper wheel method

TABLE 1

OBSERVATIONAL PARAMETERS

Frequency (GHz)	FWHM	Main Beam Efficiency	Receiver Noise Temperature (K)	τ	Spectral Resolution (km s^{-1})
115.....	21″	60%	240 SSB	0.1–0.3	2.6
230.....	13	45	260 SSB	0.2–0.4	1.3

TABLE 2

^{12}CO MAPS OF NGC 6764

LINE	MAP NUMBER	OFFSET RANGE		GRID SPACING
		Along P.A.	Perpendicular to P.A.	
^{12}CO(1–0).....	I	+20″ to −20″	−20″ to +20″	10″
^{12}CO(2–1).....	II	+20 to −20	−20 to +20	10
^{12}CO(2–1).....	III	+15 to −20	−10 to +5	5
^{12}CO(2–1).....	IV	+10 to −5	−10 to +5	5
^{12}CO(2–1).....	V	+10 to −5	−10 to +10	5
^{12}CO(2–1).....	VI	+20 to −20	−20 to +20	5 at central 20 × 20, 10 elsewhere

NOTES.—The ^{12}CO(1–0) data were taken in 1987 October; the ^{12}CO(2–1) data were taken in 1988 September (II–V) and 1990 February (VI). For maps I–V the map grid was orientated at P.A. −10°. For map VI the map grid was at P.A. 0°. All positions are with reference to $\alpha = 19^h07^m01^s.2$ and $\delta = 50°51'08''$ (1950). For both rotational transitions integration times were 5 minutes per position. The final ^{12}CO(2–1) map shown in Fig. 2 was obtained by combining maps II–V.

(Kutner & Ulich 1981). Pointing was checked on 3C 345 and NGC 2027 and confirmed by monitoring the line profile at the central position of NGC 6764 ($\alpha_{1950} = 19^h07^m01^s.2$, $\delta_{1950} = 50°51'08''$; Wilson & Willis 1980). For the simultaneous observations the pointing at 115 and 230 GHz agreed to within 3″. Pointing checks done between the ^{12}CO(2–1) maps as well as the comparison of the line profiles and individual maps indicate that both the relative pointing within each map and the absolute pointing between the different maps are of the order of 5″ (see also § 3.3). Table 2 lists integration times, sampling, and spatial extent of the measurements. Temperatures are given in terms of Rayleigh-Jeans main-beam brightness temperatures.

2.2. *The Near-Infrared Observations*

The broad-band J, H, K images were taken on 1988 July 25, at UKIRT using a 58 × 62 pixel InSb infrared array with an image scale of 2″.45 pixel^{-1}. This was done as part of the UKIRT service observing program. The integration time of the final co-added images in each band were about 2 minutes. After linearity corrections and dark current subtraction, the images have been flat-fielded using nearby sky images having the same exposure time as the source images. Bad pixels have been removed by spatial median filtering over 3 pixels. Calibration of the near-infrared data was accomplished by using the flux densities and apparent magnitudes in 8″ apertures on the nucleus quoted by Gezari, Schmitz, & Mead (1987) (see flux densities listed in Table 5). Flux densities at 0.0 mag are assumed to be 1629 Jy, 1021 Jy, and 676 Jy in the J, H, and K band (see also Campins, Rieke, & Lebofsky 1985). The uncertainties in the calibration amount to 0.17 mag in the $H-K$ and $J-H$ colors, and are dominated by a 17% discrepancy in the H band flux densities quoted in Gezari, Schmitz, & Mead (1987). However, the relative calibration is mainly affected by the quality of the flat-field corrections and results in a color uncertainty of probably less than 0.05. Before calculating the colors the position of the nucleus and the two bright stars south of the nucleus were checked. The relative center positions of the three images agreed to within less than 1 pixel.

3. RESULTS

3.1. *The Millimeter Data*

3.1.1. *Map of CO Line Emission*

Figures 2 and 3 show maps of the ^{12}CO(1–0) and ^{12}CO(2–1) line emission near the nucleus of NGC 6764. The ^{12}CO(2–1)

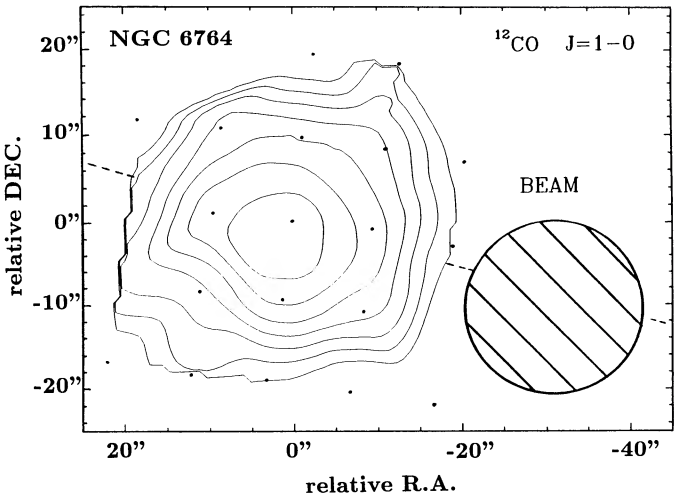

FIG. 2.—Contour map of the ^{12}CO(1–0) emission of the nuclear region of NGC 6764. Black dots indicate the position at which measurements were taken. Contour lines are 4, 8, 12, 16, 20, 24, and 28 K km s^{-1}. The peak brightness is 25 K km s^{-1}. The thin dashed line indicates the orientation of the stellar bar.

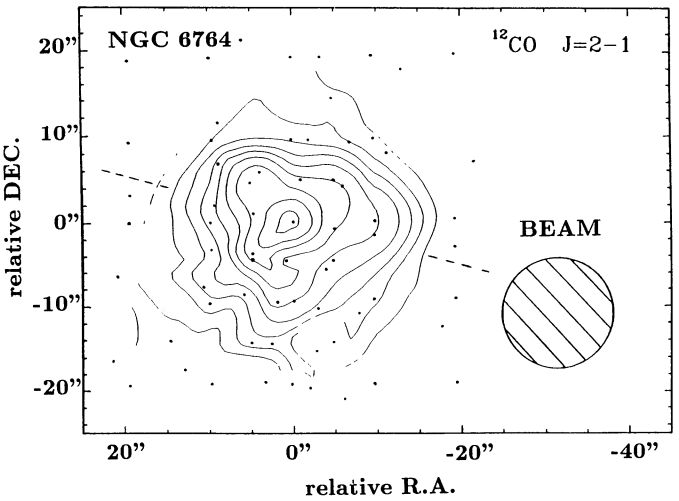

FIG. 3.—Contour map of the ^{12}CO(2–1) emission of the nuclear region of NGC 6764. Black dots indicate the positions at which measurements were taken. Contour lines are 4, 8, 12, 16, 20, 24, 28, 32, and 36 K km s^{-1}. The peak brightness is 35 K km s^{-1}. The thin dashed line indicates the orientation of the stellar bar.

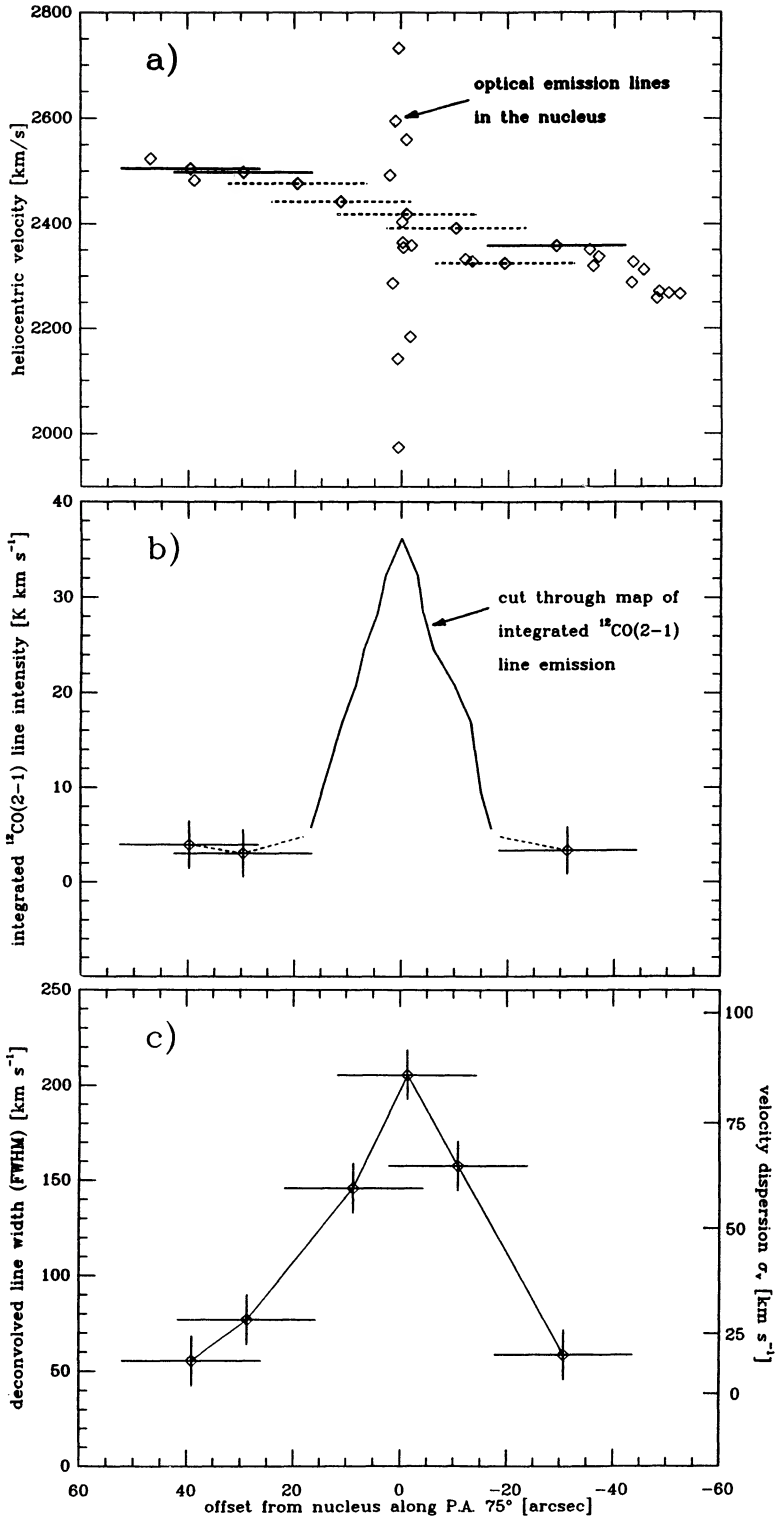

FIG. 4.—(*a*) Rotation curve of NGC 6764. We show a combination of the optical data taken by Rubin et al. (1975; see text for comment) indicated by the open diamonds and our ^{12}CO(2–1) data represented by black diamonds and horizontal bars indicating the 230 GHz beamwidth (FWHM). The dotted bars indicate data from the map; the solid lines represent the additional deep integrations on the spiral bar. (*b*) Integrated ^{12}CO(2–1) line intensity along the bar. Data in the mapped region is represented by the solid line. The estimated error in the line flux density is of the order of 10%. (*c*) ^{12}CO(2–1) line width along the bar. The line widths are corrected for the contribution of the finite beam size and the almost linear rotation curve. On the right side the velocity dispersion σ_v is plotted (see text).

map has been obtained by averaging five different maps listed in Table 2. In the emission of both lines the nucleus of NGC 6764 is only marginally resolved. Both the ^{12}CO(2–1) and ^{12}CO(1–0) map show evidence for extended emission along the bar (position angle 70°–80° east of north). Correcting for the 115 GHz and 230 GHz beamwidths, we derive an intrinsic source size of about 20″ (2.4 kpc h^{-1}) from both maps. The inner 20″ × 20″ area of the ^{12}CO(2–1) map was oversampled using a beam spacing of 5″ (about one-third of the 13″ beam). A comparison of the different maps shows that the ^{12}CO(1–0) and ^{12}CO(2–1) data sets are in excellent agreement with each other, indicating that the marginally resolved ^{12}CO(1–0) structure is probably almost the same as that seen in the higher resolution ^{12}CO(2–1) data. Observations of positions on the spiral arms NE and SW of the nucleus show that relative to the peak flux density at the central position, the flux density in the $J = 1$–0 and $J = 2$–1 lines has dropped to about 15% and 7%, respectively.

3.1.2. *Kinematics*

Because of the low spatial resolution the isovelocity contours in the central 40″ × 40″ of NGC 6764 are approximately perpendicular to the bar. The CO spectra taken on the spiral arms at distances of about 30″ and 40″ from the center show that the southwestern arm is blueshifted and the northeastern arm is redshifted with respect to the nucleus. This is in contradiction with the rotation curve published by Rubin et al. (1975). We assume that in their publication east and west are accidentally interchanged. In Figure 4*a* we show the corrected rotation curve, now also including our CO data. The rotation curve is almost linear, and the total velocity difference across the bar is about 250 km s^{-1}. Figures 4*b* and 4*c* show the ^{12}CO(2–1) line intensity and line width along the bar. For a Gaussian beam and velocity dispersion and a linear rotation curve, we can correct the observed line width for the velocity contribution per beam expected from the rotation curve. The velocity gradient across the bar is about 3 km s^{-1} arcsec^{-1}, which results in a contribution $\delta V_{\rm beam}$ to the full line width at half-maximum $\delta V_{\rm line}$ in the 13″ 230 GHz beam of about 39 km s^{-1}. An upper limit of the velocity dispersion $\sigma_{V,\rm upper}$ can then be calculated via

$$\sigma_{V,\rm upper} = \left[\frac{(\delta V_{\rm line})^2 - (\delta V_{\rm beam})^2}{8 \times \ln(2)}\right]^{1/2}. \quad (1)$$

This gives rise to the velocity dispersion scale plotted on the right-hand side of Figure 4*c*. The values for $\sigma_{V,\rm upper}$ also contain contributions from streaming motions as they are expected in strong barred potentials. The velocity dispersion is a strong function of position along the bar. It is highest at the center and decreases symmetrically toward the tips of the bar. This qualitative agreement between our observational data and nondissipative calculations of stellar bars (e.g., Miller & Smith 1979) indicates that, at least to some extent, the molecular clouds behave like gravitationally nondissipative, interacting masses. On the other hand, dissipative cloud collisions are probably a dominating mechanism that concentrates a large amount of molecular gas in the nuclear region of NGC 6764 (Pfenniger & Norman 1990).

3.1.3. *Line Ratios*

The physical condition of the molecular gas can be investigated by analyzing the ratios between the rotational transitions of isotopic CO. For the central position we can derive source size–corrected line ratios using the source size obtained directly from the millimeter data. For the arms we assume that the CO emission in each beam originates from a bar having a Gaussian cross section with a half-power width of about 15″ in one direction and (in view of the limited beam size) an infinite extent in the other direction. These assumptions are in agreement with the structure shown in the near-infrared continuum images. Table 3 lists the flux densities of the ^{12}CO and ^{13}CO $J = 2$–1 and $J = 1$–0 lines as well as the derived ratios and source size-correction (SSC) factors used.

In order to study the ^{12}CO(2–1)/^{12}CO(1–0) line ratio as a function of position, we convolved the ^{12}CO(2–1) map to the resolution of the $J = 1$–0 map. Since the maps were not taken simultaneously, we applied the following procedure to check on the relative pointing between maps: we calculated the two-dimensional, cross-correlation function between both maps in

TABLE 3

CO Isotopic Lines and their Ratios at the Center and on the Arms of NGC 6764

Parameter	Center	Arms in Map Region	Arms		
			30″ NE	40″ NE	30″ SW
^{12}CO(1–0)[b]	25 ± 2	[a]	4.7 ± 0.4	3.5 ± 0.3	3.4 ± 0.3
12CO(2–1)	35 ± 3	[a]	1.8 ± 0.2	3.0 ± 0.3	2.7 ± 0.3
^{13}CO(1–0)	1.5 ± 0.2	...	...	...	...
^{13}CO(2–1)	2.4 ± 0.3	...	...	...	...
$\left(\frac{^{12}\rm CO(2-1)}{^{12}\rm CO(1-0)}\right)_{\rm map}$	≈0.9	≈0.5	...	...	...
Observed 115 GHz size	20″ × 20″	...	15″ × ∞	15″ × ∞	15″ × ∞
Source size correction (SSC) for ratio	0.70	0.63	0.63	0.63	0.63
$\left(\frac{^{12}\rm CO(2-1)}{^{12}\rm CO(1-0)}\right)_{\rm SSC}$	1.0 ± 0.2	0.6 ± 0.1	0.2 ± 0.1	0.5 ± 0.1	0.5 ± 0.1
$\left(\frac{^{13}\rm CO(2-1)}{^{13}\rm CO(1-0)}\right)_{\rm SSC}$	1.1 ± 0.3	...	...	...	...
$\left(\frac{^{12}\rm CO(1-0)}{^{13}\rm CO(1-0)}\right)_{\rm SSC}$	18 ± 4	...	...	...	...

[a] See contour maps in Figs. 2 and 3.

[b] In the first four rows, flux densities $\int T_{\rm mb}\, dv$ are given in K km s^{-1}.

steps of 5″ and computed for each offset the ratio between maps as well. If—as indicated by the source size–corrected ratio at the central position—the CO line emission originates in moderately warm, optically thick molecular gas, the distribution of molecular line emission in the $J = 1$–0 and $J = 2$–1 line will be quite similar (see also IC 342; Eckart et al. 1990b). Therefore the cross-correlation serves as a check on the absolute positional agreement between both maps.

In addition, differences between the extreme values in the line ratio maps will be large if the positional agreement is bad. As expected, we found that the cross-correlation was highest at the assumed correct relative position between the maps, and the difference between extreme values in the quotient maps was smallest at that position as well. We therefore assume the quotient maps (Fig. 5) calculated for no relative offset between the ^{12}CO(2–1) and ^{12}CO(1–0) map to be the most reliable line ratio map that can be obtained from our data. At the center the ^{12}CO(2–1)/^{12}CO(1–0) ratio is 0.9 and drops toward the arms to a value of 0.5. Both values are consistent with those we obtain (see Table 3) using the line flux densities at the central position and in the arms and applying the previously described source size correction.

For the central position the ratio indicates emission from moderately warm, dense, optically thick gas ($T_{\rm kin} > 20$ K, $n \geq 2 \times 10^4$ cm^{-3}; see also Eckart et al. 1990b). For the arms the ratios are of the order of 0.5, indicating either low temperatures ($T_{\rm kin} \leq 10$ K) or densities too low to thermally populate the $J = 2$ rotational level. The source size–corrected ^{13}CO(2–1) to ^{13}CO(1–0) ratio equals 1.1 ± 0.2 and additionally suggests that the isotopic emission is also due to moderately warm, optically thick gas. The ^{12}CO(1–0) to ^{13}CO(1–0) ratio is about 18 ± 4. This ratio is close to the upper limit of the range of ratios found for external galaxies by Young & Sanders (1986) and Rickard & Blitz (1985).

3.2. *Near-infrared Data*

Figure 6 shows a smoothed K-band image of NGC 6764. The J-band and H-band images show similar structural features: a bar, an elongated nuclear bulge, and a bright central component. In the nonsmoothed, near-infrared images the brightness of the spiral arms is at a level of about 1%–2% of the peak core brightness. Most of the near-infrared luminosity is concentrated in a single pixel (2.″45 across) consistent with the width of the stellar optical continuum source of 1.″6 reported by Rubin et al. (1975).

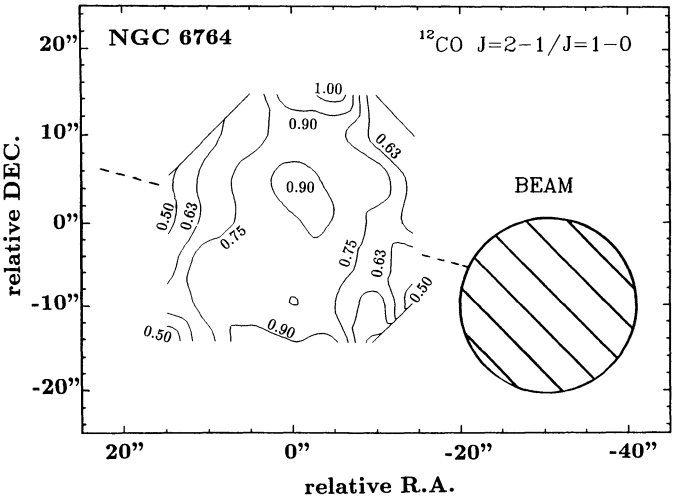

FIG. 5.—Map of the ^{12}CO(2–1) to ^{12}CO(1–0) integrated line ratio. The ^{12}CO(2–1) map has been convolved to the 115 GHz resolution (see text for further comments). The thin dashed line indicates the orientation of the stellar bar.

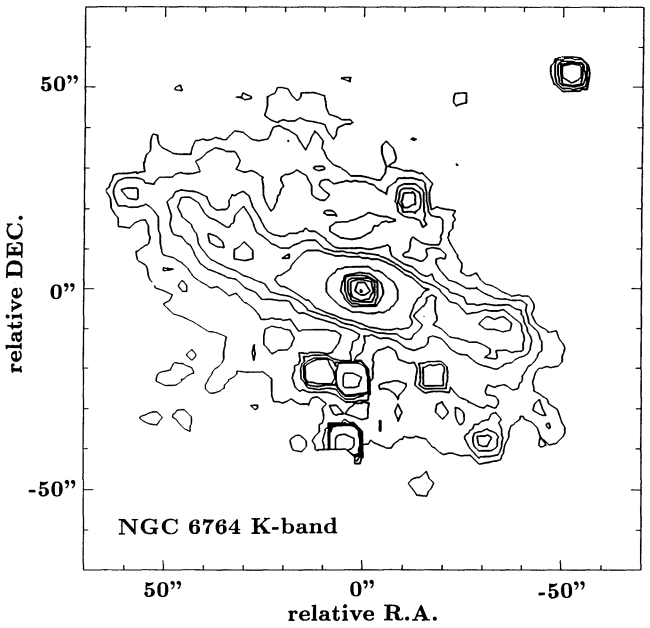

FIG. 6.—K-band map of NGC 6764 smoothed to a spatial resolution of about 7″. Contour intervals are 1.5, 3, 5, 6.5, 8, 17, 33, 45, 60, 75, 90, and 100% of the peak brightness.

In Figure 7 we show the colors for a number of representative positions in NGC 6764 and compare them to the colors of late-type stars, Sc galaxies (Scoville et al. 1985), H II-, Seyfert 1, and Seyfert 2 galaxies (Glass & Moorwood 1985). Throughout the spiral bar the colors are fairly constant with $\langle J-H \rangle = 0.6$ and $\langle H-K \rangle = 0.2$. The nucleus departs considerably from this and is much redder with $\langle J-H \rangle = 1.4$ and $\langle H-K \rangle = 0.9$. The near-infrared properties of NGC 6764 are in agreement with those found for the disks and nuclei of Seyfert 2 and H II galaxies (Glass & Moorwood 1985). A further discussion of the morphology and the near-infrared colors is given in §§ 4.5 and 4.6.

4. DISCUSSION

4.1. *Molecular Excitation*

In the following section we present simple "one-component" models of the molecular gas, which assume that the emission of the ^{12}CO and ^{13}CO isotopes all arise in regions with the same physical conditions. In an alternative "two-component" model, the ^{12}CO emission would originate from a small amount of warm, low-density molecular gas in photodissociation regions and/or a warm interclump medium in star-forming regions. The bulk of the molecular material will not be influenced by this small amount of warm gas, and the ^{13}CO emission then measures the cold (≈ 15 K) and dense ($\approx 10^4$ cm^{-3}) molecular gas contained in the clumps (see Genzel et al. 1990 and Eckart et al. 1990b for more detailed discussion).

In order to obtain more quantitative results on the molecular excitation in the simple one-component case, we calculated

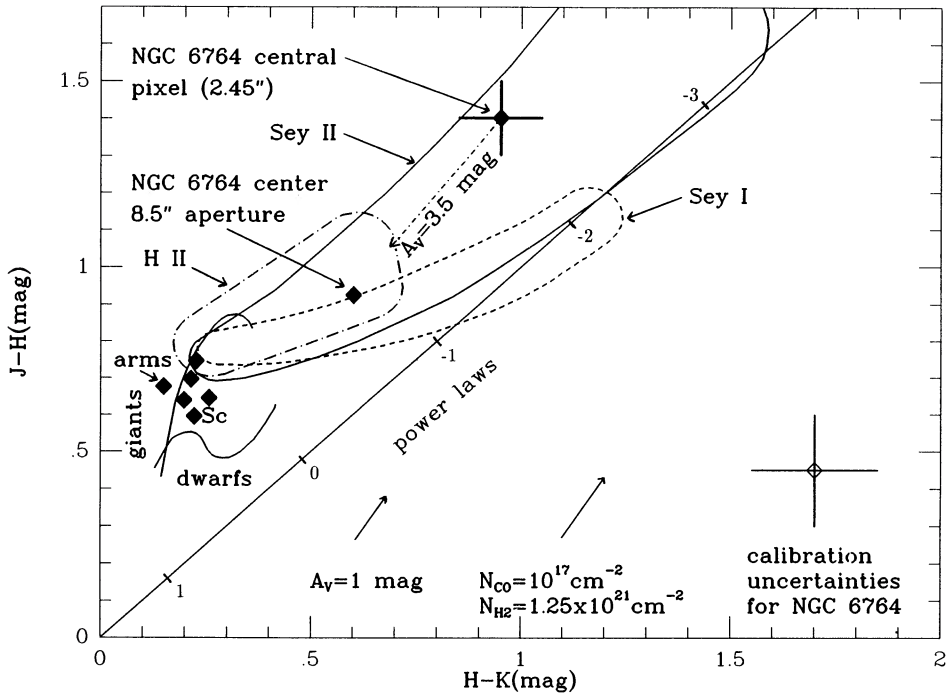

FIG. 7.—Near-infrared color as a function of position in NGC 6764 (*filled diamonds*). The error bars for the colors of the central pixel represent an estimate of the color uncertainties due to a possible misalignment between the *JHK*-images of half a pixel. Dereddening of the central pixel colors for $A_V = 3.5$ mag is indicated (see text). For comparison we show mean color sequences for giant and dwarf late-type stars (solid lines are labeled "giants" and "dwarfs"; Frogel et al. 1978) and envelopes of multiaperture data for Seyfert and H II galaxies (Glass & Moorwood 1985; apertures decrease in size toward the upper right). We also show colors for Sc galaxies (labeled "Sc"; Scoville et al. 1985). The reddening vector is taken from Cohen et al. (1981; see text). The straight line represents the location of power-law spectra in this diagram with some exponents of power laws labeled.

radiative transfer models consisting of two steps. First, we compute the populations of the 10 lowest rotational levels of ^{12}CO and ^{13}CO as a function of kinetic temperature, molecular hydrogen density, and CO column density. We assumed statistical equilibrium and fractional abundances as they are commonly found and quoted for dense molecular clouds in the Galaxy (Millar & Freeman 1984; Graedel, Langer, & Frerking 1982; Wannier 1980): $[^{12}CO]/[H_2] = 8 \times 10^{-5}$, $[^{12}CO]/[^{13}CO] = 60$. Second, we assumed a clumpy cloud model following Martin, Sanders, & Hills (1984). The model calculations are calibrated by comparing the predicted flux of the optically thinnest available isotopic line [$^{13}CO(1–0)$] to its observed flux. Kinetic temperature, number density, and column density of the molecular gas are constrained by both the line ratios given in Table 3 (especially those including ^{13}CO data) and the comparison of predicted to measured line intensity. The resulting "best physical parameters" for the nucleus of NGC 6764 can be described as follows. The beam-averaged CO column density is of the order of 2.5×10^{17} cm^{-2}, the hydrogen densities are in the range 3×10^3–3×10^4 cm^{-2}, and the minimum kinetic temperatures are between 10 and 20 K. The optical depths of the molecular clouds are about 10 for the $^{12}CO(1–0)$ line and 0.3 for the $^{13}CO(1–0)$ line.

In the galactic center molecular clouds one finds the fractional abundance of ^{13}CO to be larger by about a factor of 2 than the value for molecular clouds in the galactic disk (Wannier 1980). Therefore, we repreated the above model calculations using abundances of $[^{12}CO]/[H_2] = 8 \times 10^{-5}$, and $[^{12}CO]/[^{13}CO] = 30$ (Wannier 1980). Under these conditions the "best physical parameters" are a CO column density of 2.2×10^{17} cm^{-2}, densities of about 3×10^4 cm^{-3}, and a kinetic temperature of the order of 20 K.

For the arms we only measured the two lower rotational transitions of ^{12}CO. The source size–corrected $^{12}CO(2–1)/^{12}CO(1–0)$ ratios is of the order of 0.5 (Table 3). These low ratios exclude the possibility of emission from optically thin, thermalized, and warm molecular gas. For optically thick molecular gas the critical hydrogen density to thermalize the ^{12}CO $J = 2$ level is lower than in the optically thin case ($n_{crit(J=2)} = 2 \times 10^4$ cm^{-3}). This indicates that if the molecular gas in the arms of NGC 6764 has densities of the same order as for the nuclear region, the low $^{12}CO(2–1)$ to $^{12}CO(1–0)$ ratio can be interpreted as being due to temperatures below 10 K. However, without further isotopic data we cannot exclude the possibility of emission from warm, subthermally excited molecular gas.

4.2. *Molecular Hydrogen Masses*

In the following section we show that the total H_2 mass in the nucleus and the bar ranges between 2×10^8 and 6×10^8 $M_\odot$. In order to determine the molecular hydrogen mass more accurately, extensive data on the spatial distribution of isotopic CO and far-infrared continuum emission are required.

Estimates of the molecular hydrogen mass in NGC 6764 can be derived using the beam-averaged column density obtained from our one-component radiative transfer model calculations or from a "standard" conversion factor between the hydrogen column density and the integrated ^{12}CO intensity. However, neither method is completely satisfactory. Our data allow model calculations only for the nucleus, and even there physical conditions are probably complicated enough that multicomponent models would be more appropriate and would result in different column densities. On the other hand, the conversion factor derived for dense molecular clouds in the

Galaxy may not at all be applicable in external galaxies (Rickard & Blitz 1985; Maloney & Black 1988). In addition, one-component model calculations for different positions in IC 342 (Eckart et al. 1990b) and M82 (Wild et al. 1991) show that the conversion factor varies by at least a factor of 2 within the nuclear region of these galaxies. Since the physical properties of the molecular material in the nucleus and the bar may be different, we now describe the various methods to estimate the molecular gas masses for both components. The results are listed in Table 4.

4.2.1. *Molecular Mass of the Nucleus*

The beam-averaged ^{12}CO column density of 2.5×10^{17} cm^{-2} derived from our model calculations results in an average molecular hydrogen column density of about 3×10^{21} cm^{-2}. Assuming that this number is valid over the whole nuclear region, we can calculate a molecular hydrogen mass. The nucleus extends over an area of about 5 kpc^2 h^{-2}, resulting in a molecular hydrogen mass of about 2.4×10^8 h^{-2} $M_\odot$ (case 1 in Table 4). For higher fractional isotopic abundances the beam-averaged CO column density is only about 10% lower and results in a molecular mass of about 2.1×10^8 h^{-2} $M_\odot$ (case 2 in Table 4).

These values can be compared to the mass we obtain using the most recent, commonly adopted conversion factor between molecular hydrogen density and integrated ^{12}CO line intensity of $N(H_2)/I[^{12}CO(1–0)]$ based on γ- and millimeter radio data of about 2×10^{20} cm^{-2} K^{-1} km^{-1} s (Strong et al. 1989; case 3 in Table 4). The resulting mass using this conversion factor is 3×10^8 h^{-2} $M_\odot$, which is to within less than a factor of 2 in agreement with the molecular mass previously derived from our one-component model calculations using fractional abundances commonly found in dense molecular clouds in the Galactic disk.

4.2.2. *Molecular Mass of the Bar*

We can also estimate the molecular mass in the bar of NGC 6764. Assuming that the bar has a width of about 15″ in its CO emission, and that the total length of the bar *excluding* the nuclear region discussed above is about 75″, we can use the average CO line flux measured on the bar and calculate its molecular hydrogen mass. Using the conversion factor of 1.3×10^{20} cm^{-2} K^{-1} km^{-1} s, derived for the nucleus from our model calculations, an average ^{12}CO(1–0) line intensity of 3.9 K km s^{-1} per beam, and a beam dilution correction factor of 0.63, we find a molecular hydrogen mass of about 1.6×10^8 h^{-2} $M_\odot$ (case 4 in Table 4). The conversion factor of 2×10^{20} cm^{-2} K^{-1} km^{-1} s results in a molecular hydrogen mass of about 2.5×10^8 h^{-2} $M_\odot$ (case 5 in Table 4).

A further estimate of the molecular gas mass in the arms of NGC 6764 can be obtained by assuming the presence of cirruslike clouds in NGC 6764. Emission from cirrus clouds can account for a substantial fraction of the 100 μm continuum emission in galaxies (Helou 1986) and is known to be linked with H I 21 cm and diffuse CO emission (e.g., de Vries, Heithausen, & Thaddeus 1987). A comparison of the H I (van Gorkom 1987), ^{12}CO(1–0) line, and the 100 μm continuum emission in Centaurus A has revealed strong evidence for the fact that part of the emission can be explained by an extended component of cirruslike clouds (Eckart et al. 1990a). For barred spirals the H I emission originates predominately in the bar, spiral arms, and from regions just outside the spiral arms (Ondrechen & van der Hulst 1989; Ondrechen, van der Hulst, & Hummel 1989). If a large fraction of the molecular gas in the arms is associated with cirrus clouds, the conversion factor $N(H_2)/I[^{12}CO(1–0)]$ may be substantially lower than 2×10^{20} cm^{-2} K^{-1} km^{-1} s. Cox, Krügel, & Mezger (1986) and de Vries et al. (1987) give a factor of about 0.5×10^{20} cm^{-2} K^{-1} km^{-1} s. This conversion factor results in a molecular mass of the order of 10^8 $M_\odot$ (case 6 in Table 4). The molecular gas mass in the spiral arms would then represent only a minor fraction of the total molecular gas mass in NGC 6764.

4.2.3. *Total Neutral Atomic and Molecular Gas Mass*

Table 4 indicates that most of the molecular gas mass (>50%) is located in the nuclear region of NGC 6764 (assuming that the conversion factor in the bar is not substantially larger than that in the nucleus). The range of total molecular gas mass in the nucleus and the bar of 2–6 $\times$ 10^8 $M_\odot$ is in reasonable agreement with the initial estimate of molecular mass of 1.7×10^9 h^{-2} $M_\odot$ derived by Sanders & Mirabel (1985) from their first detection of ^{12}CO(1–0) in NGC 6764 in a 60″ beam using a conversion factor of $N(H_2)/I[^{12}CO(1–0)] = 3.6 \times 10^{20}$ cm^{-2} K^{-1} km^{-1} s. Lower conversion factors between 1–2 $\times$ 10^{20} cm^{-2} K^{-1} km^{-1} s as listed in Table 4 would result in a mass estimate close to the upper limit of our range.

Shostak (1978) and Heckman et al. (1978) found an atomic hydrogen mass of 2×10^9 h^{-2} $M_\odot$, indicating that molecular

TABLE 4

PHYSICAL PARAMETERS OF THE MOLECULAR GAS IN NGC 6764

CASE	SOURCE COMPONENT	FRACTIONAL ABUNDANCES $\frac{[^{12}CO]}{[H_2]}$	FRACTIONAL ABUNDANCES $\frac{[^{12}CO]}{[^{13}CO]}$	T_{kin} (K)	n_{H_2} (cm^{-3})	N_{CO} (cm^{-2})	PRESSURE $n_{H_2} T_{kin}$ (cm^{-3} K^{-1})	$\frac{N_{H_2}}{I^*_{CO}}$ (cm^{-2} K^{-1} km^{-1} s)	AREA (kpc^2 h^{-2})	M_{H_2} ($M_\odot$ h^{-2})
1.....	Center	8×10^{-5}	30	≈20	≈3×10^4	2.2×10^{17}	6×10^5	1.2×10^{20}	$5h^{-2}$	2.1×10^8
2.....	Center	8×10^{-5}	60	10–20	3×10^3–3×10^4	2.5×10^{17}	3×10^4–6×10^5	1.3×10^{20}	$5h^{-2}$	2.4×10^8
3.....	Center	...	...	>10	$\geq 2 \times 10^4 \beta$	...	$\geq 2 \times 10^5$	2×10^{20}	$5h^{-2}$	3×10^8
4.....	Arms	...	...	<10	≈$2 \times 10^4 \beta$	...	$<2 \times 10^5$	1.3×10^{20}	$15h^{-2}$	1.6×10^8
5.....	Arms	...	...	<10	≈$2 \times 10^4 \beta$	...	$<2 \times 10^5$	2×10^{20}	$15h^{-2}$	2.5×10^8
6.....	Arms	...	...	<10	≈$2 \times 10^4 \beta$	...	$<2 \times 10^5$	0.5×10^{20}	$15h^{-2}$	0.6×10^8

NOTES.—For cases 1 and 2 the conversion factor $N_{H_2}/I^*[^{12}CO(1–0)]$ has been derived using the model calculations described in the text. For cases 3–6 the choice of the conversion factor is described and referenced in the text. For completeness we have entered rough estimates of the kinetic temperature T_{kin} and the molecular hydrogen density n_{H_2} for cases 3–6. They result from the fact that for the nucleus, the isotopic line ratios indicate that the emission arises in moderately dense, warm, and thermalized molecular gas, whereas for the arms the ratios suggest that the gas is cold and subthermally excited. 2×10^4 cm^{-3} β is the critical density to populate the $J = 2$ level; β is the escape probability. Area and M_{H_2} are given as a function of $h = H_0/(100$ Mpc km^{-1} s).

and atomic hydrogen masses in NGC 6764 are of the same order of magnitude. The total mass of neutral atomic and molecular gas then amounts to about $3 \times 10^9\ h^{-2}\ M_\odot$. Both authors have derived a dynamical mass of approximately $6 \times 10^{10}\ h^{-1}\ M_\odot$, which is about a factor of 20 larger than the total gas mass.

4.3. *Dust Mass and Temperature*

NGC 6764 is contained in the *IRAS* point source catalog (see Table 5). The *IRAS* fluxes are listed along with the radio and near-infrared data in Table 5. From the 60 μm and 100 μm data we calculate a dust color temperature of 37 K, derived assuming an emissivity proportional to λ^{-1}. This value is in agreement with the correlation between the $^{12}CO/^{13}CO$ ratio and the dust temperature found by Young & Sanders (1986). Following Hildebrand (1983), we can derive the mass of dust in $M_\odot$ as

$$M_{\rm dust} = 4.5 D^2 F_{100} (e^{144/T} - 1)\ , \qquad (2)$$

with F_{100} being the 100 μm flux density in janskys, T the color temperature in kelvins, and D the distance in megaparsecs. For $F_{100} = 11.5$ Jy and $T = 37$ K we find a dust mass of $M_{\rm dust} = 1.4 \times 10^6\ h^{-2}\ M_\odot$. This is about a factor of 20 less than the amount of dust implied by the CO emission assuming a canonical gas to dust ratio of 100. Several factors may be responsible for the large apparent gas to dust ratio obtained above. The temperature used to determine the dust mass is calculated from the ratio of the *integrated* 60 and 100 μm fluxes for NGC 6764. If, as in the case of Centaurus A (Eckart et al. 1990a), the dust temperature decreases with increasing distance from the dust lane, the assumption of a single dust temperature may not be appropriate. In any case, *IRAS* data are insensitive to the presence of cold dust ($T \leq 10$ K) which is known to be present in substantial quantities in the Galaxy and is indicated by the fact that the kinetic temperature of the bulk of the molecular gas is of the order of 10–20 K. The existence of cold dust will lead to a larger dust mass. When these considerations are taken into account, the gas to dust ratio may be closer to the value determined for the Galaxy.

4.4. *Star Formation Rate and Efficiency*

We find strong evidence that the currently observed star formation activity in the nucleus of NGC 6764 occurs in a very intense burst which lasts probably much less than 6×10^7 yr. The star formation rate (SFR) in the nucleus is comparable to the present-day SFR in our entire Galaxy, and the global $L_{\rm FIR}/M_{\rm H_2}$ ratio is in agreement with moderate starburst activities.

4.4.1. *The Global $L_{\rm FIR}/M_{\rm H_2}$ Ratio*

The FIR luminosity of galaxies is usually interpreted as a measure of the number of visible and UV photons, which is in turn linked to the number of high-mass stars. The CO luminosity traces the amount of cool gas which is available for star formation. Therefore the ratio between FIR and CO luminosity is proportional to the star formation efficiency (SFE).

FIR luminosity can be derived using the 60 and 100 μm *IRAS* flux densities. Following the formalism given Lonsdale et al. (1985) and Fairclough (1985), we find $L_{\rm FIR} = 10^{9.82}\ h^{-2}\ L_\odot$. Combined with the range of total molecular masses of $2\text{–}6 \times 10^8\ M_\odot$ derived earlier, this results in a ratio $L_{\rm FIR}/M_{\rm H_2}$ ranging between 6 and 33 $L_\odot/M_\odot$. This is consistent with the value $12 \pm 3\ L_\odot/M_\odot$ derived for isolated, noninteracting galaxies (Young & Sanders 1986) and is smaller than 78 ± 16 $L_\odot/M_\odot$ found for mergers and interacting galaxies (Young & Sanders 1986). We therefore conclude that the overall $L_{\rm FIR}/M_{\rm H_2}$ for NGC 6764 is consistent with values for galaxies showing starburst activities. However, it is still within the range of values found for bright radio spirals (Sanders & Mirabel 1985) and close to the range of 1–10 $L_\odot/M_\odot$ found for giant molecular clouds (GMCs) in our Galaxy (Solomon & Sage 1988).

The presence of a large number of young stars at the center and the fact that the J, H, K images show the near-infrared luminosity highly concentrated toward the nucleus indicate that the bulk of the FIR luminosity may originate from the nuclear region. Since the molecular mass in this region is comparable to that contained in the bar, the $L_{\rm FIR}/M_{\rm H_2}$ ratio for the nucleus could then be up to a factor of 2 higher than the global value, and this ratio would then be well within the range of values found for interacting galaxies. In the case of NGC 6764 it is possible that instead of a recent merger or interaction with a galactic companion, streaming motions of molecular and atomic gas triggered by the bar lead to enhanced cloud collisions in the nuclear region and therefore to an enhanced SFR and SFE. This scenario would also require that the $L_{\rm FIR}/M_{\rm H_2}$

TABLE 5

RADIO AND INFRARED FLUX DENSITIES OF NGC 6764

Wavelength λ	Beam or Aperture	Flux Density (mJy)	References	Comments
21 cm	9.7	190	1	
6 cm	...	44 ± 5	2	VLA integrated map flux central 20″ × 20″
	2.7	47 ± 8	3	NRAO 91 m
	2.5	49 ± 5	4	MPIfR 100 m
100 μm	$\approx 3'$	11470	5	*IRAS*
60 μm	$\approx 2'$	6410	5	*IRAS*
25 μm	$\approx 2'$	1340	5	*IRAS*
12 μm	$\approx 1'$	380	5	*IRAS*
10.6 μm	5″	150 ± 21	6	
3.6 μm	8″	11 ± 1	6	
2.2 μm	8″	16.6 ± 0.6	6, 7	Fluxes from both references averaged
1.6 μm	8″	17.3 ± 2.3	6, 7	Fluxes from both references averaged
1.25 μm	8″	13.2 ± 0.6	6, 7	Fluxes from both references averaged

NOTES.—(1) Heckman et al. 1978. (2) Wilson & Willis 1980. (3) Sramek 1975. (4) Krichbaum, private communication. (5) Lonsdale et al. 1985. (6) Rieke 1978. (7) Aaronson et al. 1982.

ratio for the arms is then close to values found for molecular clouds in the Galaxy.

4.4.2. *Nuclear Star Formation Rate*

For the nucleus Osterbrock & Cohen (1982) find that the number of O stars derived from the Hα line flux is of the order of a few times 10^3 and equals approximately the number of Wolf-Rayet stars determined from the equivalent width of the 466 nm Wolf-Rayet feature. They argue that the total ionization in the nucleus of NGC 6764 could be accomplished by the Wolf-Rayet stars only and that the number of actual O stars could be much smaller. Assuming a stellar mass of about 30 $M_\odot$ and a lifetime of 3×10^5 yr for H II regions, we derive an approximate massive star formation rate of $dM/dt(\mathrm{OBA}) = 0.2\, M_\odot\, \mathrm{yr}^{-1}\, h^{-2}$.

This value, however, can only be a lower limit, since the optical line emission is almost certainly affected by extinction. Following Thronson & Telesco (1986), we can derive the nuclear SFR from the far-infrared luminosity. This value is less likely to be affected by absorption. Thronson & Telesco (1986) find for the formation rate of young, massive stars $dM/dt(\mathrm{OBA}) = 2.1 \times 10^{-10}\, L_{\mathrm{FIR}}\, h^{-2}$. With $L_{\mathrm{FIR}} = 10^{9.82}\, L_\odot$ this results in $dM/dt(\mathrm{OBA}) = 1.4\, M_\odot\, \mathrm{yr}^{-1}\, h^{-2}$. Assuming a Salpeter initial mass function, they obtain for the total SFR including low-mass stars $dM/dt(\mathrm{total}) = 3.1 \times dM/dt(\mathrm{OBA}) = 4.3\, M_\odot\, \mathrm{yr}^{-1}\, h^{-2}$. This indicates that the star formation rate in the nuclear region of NGC 6764 is comparable to the star formation rate of our entire Galaxy (Smith, Biermann, & Mezger 1978; Güsten & Mezger 1982).

There is even an indication that the current formation rate of young massive stars is much higher: Ulvestad (1982) calculates the minimum number and rate of recent supernovae that would be required to account for the nonthermal radio flux density of NGC 6764. He finds a number of 19 h^{-2} recent supernova remnants (SNR) and a rate of 2 h^{-2} SNR yr^{-1}. The formation rate of young, massive stars of about 1.4 $M_\odot\, \mathrm{yr}^{-1}\, h^{-2}$, as derived above, is about an order of magnitude less than that required to sustain the supernova rate derived by Ulvestad (1982), assuming a mass of about 10 $M_\odot$ per OBA star. This suggests that either the far-infrared does not measure the total SFR or that the nonthermal emission is not entirely due to supernova remnants.

A SFR of 4 $M_\odot\, \mathrm{yr}^{-1}\, h^{-2}$ and about $3 \times 10^8\, M_\odot$ of molecular gas in the nucleus of NGC 6764 lead to a lifetime for the molecular gas of approximately 6×10^7 yr. This time scale can be compared to the time that is required to refuel the molecular gas. One mechanism of refueling is stellar mass loss. In the following we adopt (1) a value for the mass-loss rate of late-type stars of $1.5 \times 10^{-11}\, M_\odot\, \mathrm{yr}^{-1}\, L_\odot^{-1}$ (Faber & Gallagher 1976); (2) a mass-loss rate for Wolf-Rayet stars of approximately $7 \times 10^{-5}\, M_\odot\, \mathrm{yr}^{-1}$ (de Freitas Pacheco & Machado 1988); and (3) a typical mass-loss rate for OB stars of $10^{-6}\, M_\odot\, \mathrm{yr}^{-1}$ (e.g., Blomme & van Rensbergen 1988). Furthermore, we assume that both the number of Wolf-Rayet and OB stars is a few times 10^3 (Osterbrock & Cohen 1982). With these numbers we find that the maximum refueling rate due to stellar mass loss in the nucleus of NGC 6764 is less than 0.5 $M_\odot\, \mathrm{yr}^{-1}$. This rate is by more than an order of magnitude smaller than the suggested current total SFR. Furthermore the structure in the radio maps (Wilson & Willis 1980; Ulvestad et al. 1981) and the morphology in our ^{12}CO maps may indicate a nuclear outflow (see § 4.5) such that the actual loss of molecular gas may consequently be much higher than 4 $M_\odot\, \mathrm{yr}^{-1}$. In addition, we can expect that the newly formed massive stars will either have a damping or amplifying influence on further formation of stars. In both cases the time over which star formation takes place will probably be shortened. The amplifying influences will lead to an enhanced SFR; the damping influences could either reduce the SFR to a value that can be sustained by the fueling mechanisms or actually stop the formation of young massive stars entirely (e.g., by fragmentation of molecular clouds by strong stellar winds; e.g., Larson 1987). This indicates that the actual duration of the starburst at the nucleus of NGC 6764 occurs in probably much less than the previously derived time of 6×10^7 yr.

4.5. *Morphology of the Nucleus*

The nuclear morphology in the CO line emission can be explained by the response of molecular gas to a barlike potential or by a nuclear outflow due to the central starburst. Higher spatial resolution and extensive information on the velocity field are needed to distinguish between both models or their contributions.

4.5.1. *Gas in the Barlike Potential*

There are structural similarities between maps of the millimeter molecular line emission and the radio and *K*-band continuum emission. The ^{12}CO(2–1) map (Fig. 3) shows two major structural components: (1) a compact core with an extension to the NE at a P.A. of 50° and (2) extended emission to the NW and SE at a P.A. of about −50 and 130°, respectively. These structural features are also indicated in the 6 cm VLA maps (Fig. 7; Ulvestad et al. 1981; Wilson & Willis 1980), suggesting that both the distribution of the dense molecular gas and the nonthermal radio emission ($\alpha_{20/6} = -1.0$; see Table 5) trace the same regions of recent, active star formation. A comparison of the intensity profiles of the *K* band and the ^{12}CO(2–1) map (Fig. 8) shows that most of the CO luminosity arises in the nuclear bulge component, showing that the nucleus itself is embedded in a compact stellar and gaseous bulge.

The distribution of the molecular gas in the center of NGC 6764 may reflect the predicted gaseous response to a barlike potential. In the Hα map (Boehr & Schulz 1990) enhanced emission along the southeastern and northwestern edge of the spiral bar is indicated. This emission may be due to H II regions of young, luminous stars formed in the shocked dust lane tracing linearly offset density enhancements at the leading edges of spiral bars with trailing spiral arms. These offset enhancements are often observed and predicted by gas dynamical calculations for strong spiral bars (e.g., Roberts, Huntley, & van Albada 1979; Sanders & Tubbs 1980). The model calculations also predict a central oval distortion in the distribution of the gas that connects the offset enhancements across the nucleus. In NGC 6764 this distortion may be represented by the extended emission to the SE and NW. However, the presence of the northeastern extension at a P.A. of 50° indicates that the situation may be more complicated.

4.5.2. *Indication for a Nuclear Outflow?*

An alternative or complementary explanation for the extended molecular emission seen towards the SE and NW is the presence of a nuclear outflow. In a few galaxies (e.g., M82, NGC 253) nuclear outflows are observed which are probably sustained by the ongoing starburst at their nuclei (e.g., Chevalier & Clegg 1985; Tomisaka & Ikeuchi 1988). These models involve hot gas with an outflow velocity of about 1000 km s^{-1} that is able to accelerate clouds out from the center of the

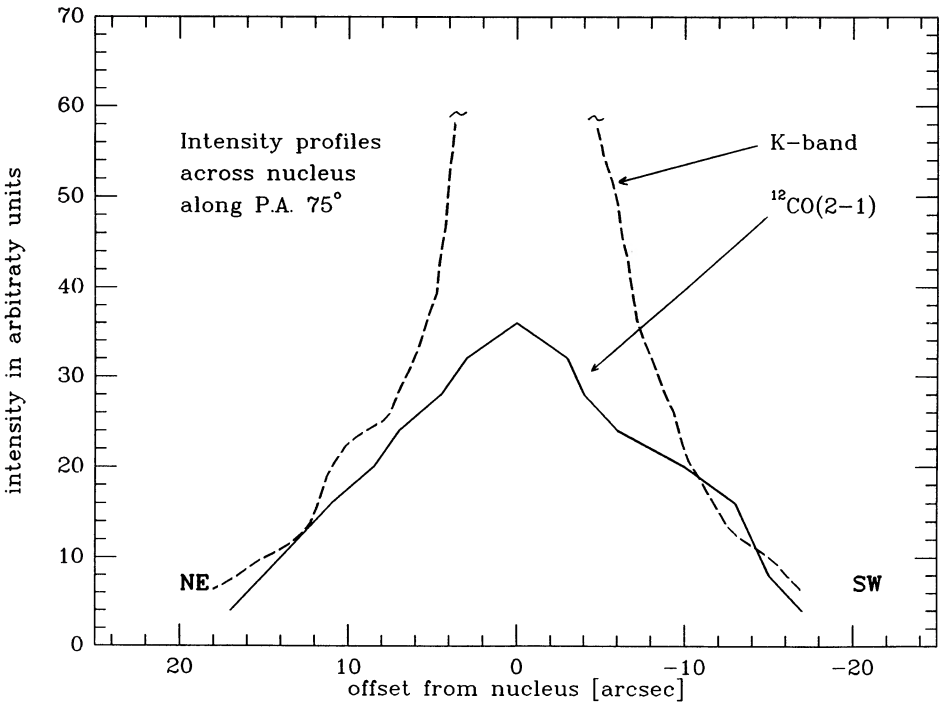

FIG. 8.—A comparison of the near-infrared continuum and the ^{12}CO(2–1) line emission intensity profiles. The CO data are taken from the map in Fig. 3. The bulk of the molecular gas is associated with a massive, barlike nuclear stellar bulge.

galaxy. Although in the case of NGC 6764 there is limited observational evidence for such a phenomenon, it is difficult to explain the large amount of molecular gas that would be involved in such an outflow.

The observational evidence can be summarized as follows: the radio structure reported by Wilson & Willis (1980) (Figure 9) and Ulvestad et al. (1981) shows strong extended emission to the southeast, at a P.A. of about 150°, i.e., almost perpendicular to the bar. Our ^{12}CO(2–1) map shows evidence for extended emission in this direction as well. Hummel et al. (1983) define a sample of spiral galaxies which appear T-shaped in the radio. For the barred spiral galxy NGC 613 (Hummel et al. 1987), which is among Hummel's sample, optical and radio observations provide strong evidence for an accelerated collimated outflow with a velocity gradient of approximately 95 km s^{-1} kpc^{-1}. Rubin et al. (1975) have shown that at the center of NGC 6764 there is evidence for systematic motion perpendicular to the bar. Assuming a symmetrical rotation curve—which is supported by our CO measurements—they find a heliocentric velocity of 2405 $\pm$ 8 km s^{-1} for the center, whereas the heliocentric velocity derived from permitted optical emission lines is 2363 $\pm$ 6 km s^{-1}. This results in a significant, systematic velocity difference of about 40 km s^{-1} for the center which could be the actual projected velocity of a nuclear outflow. The facts mentioned above give rise to the assumption that the situation in the central region of NGC 6764 may be quite similar to that in the nucleus of NGC 613.

In order to test whether an outflow is a realistic alternative for NGC 6764, we check the implied mass loss and energy balance. We assume an energy input of two supernovae per year $dE/dt = 2 \times 10^{51}$ ergs yr^{-1} (Ulvestad 1982), a deprojected flow velocity of the accelerated molecular gas of about $v_{\rm flow}$ = 100 km s^{-1}, and the amount of molecular material involved in the flow and contained in the extensions indicated in the ^{12}CO(2–1) map of $m_{\rm flow} = 10^8\ M_\odot$. The total energy available after a massive starburst of duration $t_{\rm burst} = 10^7$ yr is then $E_{\rm total} = (t_{\rm burst})dE/dt = 2 \times 10^{58}$ ergs. The energy contained in the flow is of the order of $E_{\rm flow} = 0.5(m_{\rm flow})(v^2_{\rm flow}) = 10^{55}$ ergs. This indicates that if the efficiency with which the $E_{\rm total}$ is coupled to $E_{\rm flow}$ is of the order of 10^{-3} (a value which is not unreasonable: Chevalier & Clegg 1985), the assumed supernova rate is able to sustain a massive molecular flow.

The mass-loss rate can be estimated via $dM/dt = \phi n m_{\rm H_2} v_{\rm flow} A$. A is the cross section area of the flow and is

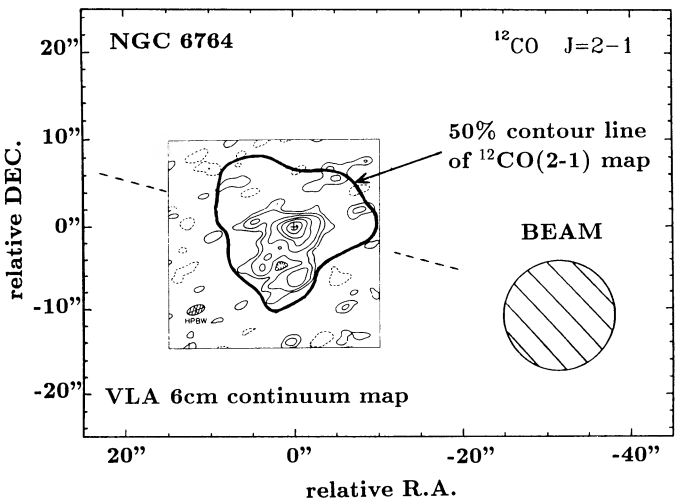

FIG. 9.—A comparison of the ^{12}CO(2–1) data with the 6 cm VLA continuum map (Ulvestad et al. 1981; Wilson & Willis 1980). At quite different resolutions both maps show strong evidence for a compact nucleus with an extension to the NE and extended emission to the SE and NW. The thin dashed line indicates the orientation of the stellar bar.

assumed to be 500 × 500 pc^2, the typical density in molecular clouds and clumps in the flow is $n = 10^3$ cm^{-3}, m_{H_2} is the mass of a hydrogen molecule, and $\phi = 10^{-2}$ is the area filling factor of the dense material in . The choice of ϕ is justified by the fact that $\phi n m_{H_2} A^{3/2}$ is of the order of the total molecular mass assumed to be involved in the flow. These values then result in $dM/dt = 1\ M_\odot\ \mathrm{yr}^{-1}$. The hot gas which is driving the flow can be assumed to have a larger filling factor and velocity but a much smaller density (1 cm^{-3} or less), such that the mass-loss rate via hot gas is probably of the order of 1 $M_\odot$ yr^{-1} as well. The total mass loss of 2 $M_\odot$ yr^{-1} can just be balanced by the mass injection from young massive stars and the assumed supernova rate (§ 4.4.2).

However, the fact, that v_{flow} is smaller than the escape velocity and the terminal velocity of clouds accelerated by the wind by a factor of a few (Chevalier & Clegg 1985), indicates that gravitational effects have to be included in a final analysis. Also, observations at a higher spatial resolution are required to study the velocity field in more detail.

4.6. *Near-infrared Colors and Extinction*

Combining our data on the molecular gas and the apparent NIR colors, and assuming that the relation

$$A_V = 5.5 \times 10^{-22}(N_{\mathrm{H\,I}} + 2N_{H_2}) \qquad (3)$$

is applicable in NGC 6764, we can obtain a first-order estimate of the extinction averaged in the millimeter-beams and calculate dereddened colors. The contribution of atomic hydrogen to the visual extinction toward the nucleus is probably negligible compared to the large amount of molecular gas (Ondrechen & van der Hulst 1989; Ondrechen et al. 1989). The nucleus is therefore only partially covered by one or several molecular cloud complexes, which in part can have high optical depths (see § 4.1). Via equation (3) we can then transform the extinction vector in Figure 7 (Cohen et al. 1981) into a vector of equivalent molecular hydrogen column density.

For the spiral arms the integrated CO intensity is less than about 1/10 of the nuclear intensity. If most of the molecular and atomic gas is distributed homogeneously *along* the offset density enhancements indicated in the Hα map (Boehr & Schulz 1990), the beam-averaged extinction in the *JHK* bands *across* most of the bar is probably less than 1 mag, and the colors of the bar will be dominated by mostly not-obscured, late-type stars. Dereddening would then shift the locations of the data points for the spiral arms in Figure 7 only by a small amount to the lower left, and the colors are still in agreement with those expected for the disk component of Seyfert and H II galaxies.

The 115 GHz–beam-averaged molecular column density N_{H_2} toward the center of NGC 6764 is of the order of 3×10^{21} cm^{-2} (Table 4; assuming a fractional abundance of $[^{12}\mathrm{CO}]/[\mathrm{H}_2] = 8 \times 10^{-5}$). The nucleus can be assumed to be in the center of the stellar and gaseous bulge such that the molecular column density between the observer and the nucleus is $\frac{1}{2}N_{H_2}$. However, Figure 2 suggests a concentration of the CO emission (and possibly also of the gas, depending on the variation of molecular excitation) toward the nucleus by at least a factor of 2.

Therefore 3×10^{21} cm^{-2} appears to be a reasonable value for the molecular column density toward the core component of NGC 6764. Even in a clumpy interstellar medium it is unlikely that the actual column density deviates significantly from this average value, since the nucleus exhibits an extent of almost 2″ (Rubin et al. 1975) corresponding to 230 pc h^{-1}, which is about 2 to 3 times the size of giant molecular cloud complexes in the Galaxy. Via equation (3) this results in an extinction of $A_V = 3$–4 mag. As is apparent from Figure 7, the dereddening places the nucleus into the region characteristic for nuclei of H II galaxies. Therefore the center of NGC 6764 could be looked at as an obscured H II galaxy nucleus. An alternative explanation is that of a composite nucleus resulting from significant contributions of both a power-law source and a stellar component. This interpretation is consistent with the analysis of optical emission-line data by Boer & Schulz (1990).

Contributions of various emission mechanisms in the near-infrared for galactic nuclei are discussed in the literature (e.g., Willner et al. 1985; Heckman et al. 1983; Balzano 1983; Lebofsky, Rieke, & Kemp 1978; Rieke 1978; Rees et al. 1969). Rees et al. (1969) have shown that a power-law spectrum can be obtained via emission from hot dust covering a broad range of temperatures. However, the exact nature of these nuclear sources is unclear. In the case of NGC 6764 we can exclude a significant contribution from free-free radiation using the relation between the Hβ and 5 GHz radio flux density given by Lequeux (1980) and the ratios of *J*, *H*, *K* to 5 GHz flux densities given by Thuan (1983). These relations indicate a contribution of free-free radiation of less than 1% to the near-infrared flux densities. Composite models making use of contributions of stars and hot dust are most likely to account for the shape of the near-infrared spectrum. These models, however, require both a better frequency coverage of the optical/infrared spectrum of NGC 6764 and maps at a higher spatial resolution.

4.7. *Comparison with Other Sources*

Table 6 compares the integrated ^{12}CO(2–1)/^{12}CO(1–0) line ratios toward the center of a variety of objects with different optical identifications. As outlined in § 4.1, this ratio provides a first insight into the physical state (number density and temperature) of the molecular interstellar medium. Therefore Table 6 can be used to search for differences between the molecular gas phase in sources with different optical classifications. If starbursts play a significant role in this evolution, we would expect to detect differences in the properties of the molecular interstellar medium. The sources selected belong to classes of objects which are believed to be linked in evolution (e.g., Norman & Scoville 1988; Sanders et al. 1988; Rieke et al. 1988). However, such a comparison suffers from the fact that in most of the cases the actual extent of the line-emitting region is not known. Furthermore, it is not possible to distinguish easily between the varying contributions of the disk and core components within the telescope beam. On the other hand, Table 6 shows that for all sources (except M82; for a detailed discussion of new measurements and published data for M82 see Wild et al. 1990, 1991) the ^{12}CO(2–1)/^{12}CO(1–0) ratios vary between 0.5 and 1.2, which is in excellent agreement with the range of line ratios one would expect for a varying disk-to-core contribution and for intrinsic line ratios of both components as obtained from the spatially resolved sources in Table 6.

This indicates that—although differences in the pressure of the interstellar medium (e.g., Eckart et al. 1990b) and the interstellar radiation field (Stacey et al. 1991; Young & Sanders 1986) between galaxies are indicated—the physical states of the molecular gas in the different sources show some common properties. In all these objects the nuclear molecular line emission is mainly originating in moderately warm and dense gas,

TABLE 6

THE ^{12}CO(2–1)/^{12}CO(1–0) RATIO TOWARDS THE CENTERS OF SELECTED GALAXIES

Source Type	Source Name	$\int T_{mb}\,dv$ ^{12}CO(1–0)	$\int T_{mb}\,dv$ ^{12}CO(2–1)	Ratio $\frac{^{12}\text{CO(2–1)}}{^{12}\text{CO(1–0)}}$	Comment
QSO	I Zw 1	7	11	1.0–1.2	Assumed component size 15–25″ (Barvainis, Alloin, & Antonucci 1989)
Seyfert 2	NGC 1068	136	...	0.7–0.9	^{12}CO(2–1) map convolved to ^{12}CO(1–0) map resolution (Planesas, Gomez-Gonzales, & Martin-Pintado 1989)
LINER	NGC 6764	27	35	0.8–1.0	^{12}CO(2–1) map convolved to ^{12}CO(1–0) map resolution (this paper)
Elliptical radio galaxy	NGC 1275 (3C 84)	25	15	$\approx$0.6	Assumed component size $\approx$40″ (Lazareff et al. 1989)
Elliptical radio galaxy	NGC 5128 (Cen A)	71	74	0.9–1.0	Assumed source size 33″ × ∞ (Phillips et al. 1989; Eckart et al. 1990a)
Starburster (Irr galaxy)	M82	11 ± 0.″3	15 ± 0.″3	1.4 ± 0.4	(Wild 1990; Wild et al. 1991 and references therein)
Sc with starburst activity	IC 342	213	324	1.0–1.2	^{12}CO(2–1) map convolved to ^{12}CO(1–0) map resolution (Eckart et al. 1990b)

NOTES.—For all sources except Centaurus A the observations have been carried out using the IRAM 30 m millimeter telescope. We have calculated the source size corrections assuming Gaussian source profiles and spatial resolutions (FWHM) of 21″ at 115 GHz and 13″ at 230 GHz. For Centaurus A observations were conducted with the Swedish-ESO-Submillimeter Telescope (*SEST*) with a spatial resolution (FWHM) of 45″ at 115 GHz and 22″ at 230 GHz. For I Zw 1 and 3C 84 a sensible range of possible source sizes was obtained by inspecting optical images of the source. All line intensities, with the possible exception of 3C 84, have been corrected for main beam efficiencies. The corresponding correction for 3C 84 would move the ratio closer to a value of 1.0. For M82 (*) we have listed the source size–corrected Rayleigh-Jean peak brightness temperatures on the southwestern lobe.

and the emission in the disk is due to cold or subthermally excited gas. The influence of warm, optically thin molecular gas on the global appearance of the different objects is minor. A more detailed comparison of the molecular interstellar media in sources of different classes has to be based on a multiline analysis of CO isotopes. Especially for the fainter and more distant objects, the data are not yet available.

The CO line emission and far-infrared properties of NGC 6764 are in agreement with statistical properties of Seyfert galaxies (Heckman et al. 1989; Blitz, Mathieu, & Bally 1986; Bieging et al. 1981; Meixner et al. 1990). As in most of the cases in which the spatial distribution of CO emission has been studied, in these sources the emission is highly concentrated at the nucleus (for NGC 6764 about 50%). The fact that this is also the case for three other barred spirals (Sandqvist, Elfhag, & Jörsäter 1988; Gerin, Nakai, & Combes 1988; Jackson et al. 1991) suggests that there must be an effective mechanism that concentrates molecular material in the nuclear regions of these objects.

5. CONCLUSIONS

The result of our investigation of the millimeter molecular line and near-infrared continuum emission in NGC 6764 can be summarized in the following points:

1. Comparing the morphologies of the near-infrared continuum and ^{12}CO line emission, we find that most of the molecular gas is associated with a massive, nuclear stellar bulge.

2. The molecular gas at the nucleus is moderately warm ($T_{\rm kin} \approx 20$ K) and dense ($n_{\rm H_2} \geq 2 \times 10^4$ cm^{-3}). The molecular gas in the spiral arms is probably cold ($T_{\rm kin} \leq 10$ K) and/or subthermally excited.

3. Estimates of the total molecular gas mass in NGC 6764 range from 2 to 6×10^8 $M_\odot$ depending on the choice of conversion factor between the integrated intensity of the ^{12}CO(1–0) line and the H_2 column density or the isotopic abundances in model calculations of radiative transfer. In any case, most of the molecular gas (>50%) is concentrated in the inner kiloparsec of the nucleus.

4. The overall $L_{\rm FIR}/M_{\rm H_2}$ ratio is consistent with values for galaxies showing starburst activities, but it is significantly smaller than values found for mergers or interacting galaxies.

5. The star formation rate in the nucleus is of the order of a few solar masses per year. Refueling arguments suggest that the duration of the burst is very short—less than 6×10^7 yr.

6. The distribution of the extended molecular gas tracted by the ^{12}CO(2–1) line emission is in agreement with the predicted response of nuclear gas to a barlike gravitational potential. An alternative explanation of this emission is the presence of a nuclear outflow almost perpendicular to the bar.

7. The near-infrared colors of the bar are in agreement with colors expected for late-type stars and Sc galaxies. Applying the beam-averaged molecular column density, we expect an extinction of $A_V = 3$–4 mag toward the extended nucleus. The dereddened nuclear colors are indicative of a composite galactic nucleus resulting from significant contributions of both a power-law source and a stellar component.

Our investigation allows us to draw two more general conclusions, which may be important for further investigation of the evolution of the molecular interstellar medium in galaxies:

1. From the comparison of the ^{12}CO(2–1)/^{12}CO(1–0) line ratios of NGC 6764 and objects of different morphological classes, we can conclude that starburst galaxies, elliptical radio galaxies, Seyfert galaxies, and quasars show some common beam-averaged properties of the molecular gas. The bulk of the nuclear molecular line emission arises in moderately warm, dense, optically thick gas (line ratio $\approx$1.0). The CO line emission in the disks and arms of the galaxies arises from cold and probably subthermally excited gas (line ratio $\approx$0.5).

2. Even though the Wolf-Rayet emission-line features are

direct evidence for recent or ongoing massive star formation, at a spatial resolution of 10–20″ this is not readily evident from the two lowest rotational transitions of ^{12}CO and ^{13}CO. The presence of large amounts of warm, optically thin gas that might be expected from active star formation regions would be indicated by line ratios significantly larger than 1 (and less than 4). This suggests that at this resolution the presence of the Wolf-Rayet feature is not strongly linked to the bulk properties of the molecular gas in the nuclei of galaxies. This may be a consequence of the compactness and small filling factor of this region.

We therefore expect that differences in the properties of the nuclear molecular material between galaxies of hypothetically different evolutionary stages may require spatial resolutions of less than 10″. This is especially true since even limited statistical samples of objects will have to cover a reasonably wide range of redshifts, resulting in small source sizes. Also, observations of higher rotational transitions of CO may be important if the objects differ significantly in the amount of warm molecular gas.

We are grateful to the 30 m telescope staff and thank IRAM for their support and hospitality. We thank T. P. Krichbaum for providing flux density measurements with the Effelsberg 100 m telescope. M. C. acknowledges the support of the Royal Society through its European Science Exchange Programme.

REFERENCES

Aaronson, M., et al. 1982, ApJS, 50, 241
Armus, L., Heckman, T. M., & Miley, G. K. 1988, ApJ, 326, L45
Balzano, V. A. 1983, ApJ, 268, 602
Barvainis, R., Alloin, D., Antonucci, R. 1989, ApJ, 337, L72
Bieging, J. H., Blitz, L., Lada, C. L., & Stark, A. A. 1981, ApJ, 247, 443
Blitz, L., Mathieu, R. D., & Bally, J. 1986, ApJ, 311, 142
Blomme, R., & van Rensbergen, W. 1988, A&A, 207, 70
Blundell, R., Carter, M., & Gundlach, K. H. 1988, Internat. J. Infrared Millimeter Waves, 9, 361
Blundell, R., Gundlach, K. H., Blum, E. J., Ibruegger, J., & Hein, H. 1985, in Internat. Symposium on Millimeter and Submillimeter Radio Astronomy (Granada: URSI), 117
Boehr, B., & Schulz, H. 1990, Ap&SS, 168, 201
Campins, H., Rieke, G. H., & Lebofsky, M. J. 1985, AJ, 90, 896
Cox, P., Krügel, E., & Mezger, P. G. 1986, A&A, 155, 380
Chevalier, R. Z., & Clegg, A. W. 1985, Nature, 317, 44
Cohen, J. G., Frogel, J. A., Persson, S. E., & Elias, J. H. 1981, ApJ, 249, 481
de Freitas Pachecp, J. A., & Machado, M. A. 1988, AJ, 96, 365
de Vries, H. W., Heithausen, A., & Thaddeus, P. 1987, ApJ, 319, 723
Eckart, A., Cameron, M., Rothermel, H., Wild, W., Zinnecker, H., Rydbeck, G., Olberg, M., & Wiklind, T. 1990a, ApJ, 363, 451
Eckart, A., Downes, D., Genzel, R., Harris, A. I., Jaffe, D. T., & Wild, W. 1990b, ApJ, 348, 434
Faber, S. M., & Gallagher, J. S. 1976, ApJ, 204, 365
Fairclough, J. H. 1985, in Extragalactic Infrared Astronomy, ed. P. M. Gondhalekhar (Rutherford Appleton Lab. Workshop, RAL-85-086), 32
Frogel, J. A., Persson, S. E., Aaronson, M., & Matthews, K. 1978, ApJ, 220, 75
Genzel, R., Stacey, G. J., Harris, A. I., Townes, C. H., Geis, N., Graf, U. U., Poglitsch, A., & Stutzki, J. 1990, ApJ, 356, 160
Gerin, M., Nakai, N., & Combes, F. 1988, A&A, 203, 44
Gezari, D. Y., Schmitz, M., & Mead, J. M. 1987, NASA Ref. Pub. 1196, Catalog of Infrared Observations, Part I—Data (2d. ed.)
Giles, A. B. 1986, MNRAS, 218, 615
Glass, I. S., & Moorwood, A. F. M. 1985, MNRAS, 214, 429
Graedel, T. E., Langer, W. D., & Frerking, M. A. 1982, ApJS, 48, 321
Güsten, R., & Mezger, P. G. 1982, Vistas Astr., 26, 159
Heckman, T. M., Balick, B., & Sullivan, W. T. III. 1978, ApJ, 224, 745
Heckman, T. M., Blitz, L., Wilson, A. S., Armus, L., & Miley, G. K. 1989, ApJ, 342, 735
Heckman, T. M., Lebofsky, M. J., Rieke, G. H., & van Breugel, W. 1983, ApJ, 272, 400
Helou, G. 1986, ApJ, 311, L33
Hildebrand, R. H. 1983, QJRAS, 24, 267
Hummel, E., Joersaeter, S., Lindblad, P. O., & Sandqvist, A. 1987, A&A, 172, 51
Hummel, E., van Gorkum, J. H., & Kotanyi, C. G. 1983, ApJ, 267, L5
Jackson, J. M., Eckart, A., Pogge, R. W., Ho, P. T. P., Wild, W., & Harris, A. I. I. 1991, ApJ, in press
Krichbaum, T. P., private communication
Kutner, M. L., & Ulich, B. L. 1981, ApJ, 250, 341
Larson, R. B. 1987, in Starbursts and Galaxy Evolution, ed. T. X. Thuan, T. Montmerle, & J. Tran Thahn Van (Gif-sur-Yvette: Editions Frontieres), 467
Lazareff, B., Castets, A., Kim, D.-W., & Jura, M. 1989, ApJ, 336, L13
Lebofsky, M. J., Rieke, G. H., & Kemp, J. C. 1978, ApJ, 222, 95
Lequeux, J. 1980, in Star Formation, ed. A. Maeder & L. Martinet (Sauverny: Geneva Observatory), 77
Lonsdale, C. H., Helou, G., Good, J. C., & Rice, W. 1985, Cataloged Galaxies and Quasars Observed in the *IRAS* Survey (Pasadena: NASA-JPL)
Maloney, P., & Black, J. H. 1988, ApJ, 325, 389
Martin, H. M., Sanders, D. B., & Hills, R. E. 1984, MNRAS, 208, 35
Meixner, M., Puchalsky, R., Blitz, L., Wright, M., & Heckman, T. 1990, ApJ, 354, 158
Millar, T. J., & Freeman, A. 1984, MNRAS, 207, 425
Miller, R. H., & Smith, B. F. 1979, ApJ, 227, 785
Norman, C., & Scoville, N. 1988, ApJ, 332, 124
Ondrechen, M. P., & van der Hulst, J. M. 1989, ApJ, 342, 29
Ondrechen, M. P., van der Hulst, J. M., & Hummel, E. 1989, ApJ, 342, 39
Osterbrock, D. E., & Cohen, R. D. 1982, ApJ, 261, 64
Pfenniger, D., & Norman, C. 1990, ApJ, 363, 391
Phillips, T. G., Sanders, D. B., & Sargent, A. I. 1990, in Proc. Symposium Submillimeter & Millimeter Astronomy (Kona, Hawaii), ed. G. D. Watt & A. S. Webster (Dordrecht: Kluwer), 223
Planesas, P., Gomez-Gonzales, J., & Martin-Pintado, J. 1989, A&A, 216, 1
Rees, M. J., Silk, J. I., Werner, M. W., & Wickramasinghe, N. C. 1969, Nature, 223, 788
Rickard, L. J., Blitz, L. 1985, ApJ, 292, L57
Rieke, G. H. 1978, ApJ, 226, 550
Rieke, G. H., Lebofsky, M. J., & Walker, C. E. 1988, ApJ, 325, 679
Roberts, W. W., Huntley, J. M., & van Albada, G. D. 1979, ApJ, 233, 67
Rubin, V. C., Thonnard, N., & Ford, W. K. 1975, ApJ, 199, 31
Sanders, D. B., & Mirabel, I. F. 1985, ApJ, 298, L31
Sanders, D. B., Soifer, B. T., Elias, J. H., Madore, B. F., Matthews, K., Neugebauer, G., & Scoville, N. 1988, ApJ, 325, 74
Sanders, D. B., Solomon, P. M., & Scoville, N. Z. 1984, ApJ, 276, 182
Sanders, R. H., & Tubbs, A. D. 1980, ApJ, 235, 803
Sandqvist, A., Elfhag, T., & Jörstäter, S. 1988, A&A, 201, 223
Scoville, N. Z., Soifer, B. T., Neugebauer, G., Young, J. S., Matthews, K., & Yerka, J. 1985, ApJ, 289, 129
Shostak, G. S. 1978, A&A, 68, 321
Smith, L. F., Biermann, P., & Mezger, P. G. 1978, A&A, 66, 65
Solomon, D. B., & Sage, L. J. 1988, ApJ, 334, 613
Sramek, R. 1975, AJ, 80, 771
Stacey, G. J., Geis, N., Genzel, R., Lugten, J. B., Poglitsch, A., Sternberg, A., & Townes, C. H. 1991, ApJ, in press
Strong, A. W., et al. 1989, Proc. 20th Internat. Cosmic Ray Conf., 1, 125
Thronson, H. A., Jr., & Telesco, C. M. 1986, ApJ, 311, 98
Thuan, T. X. 1983, ApJ, 268, 667
Tomisaka, K., & Ikeuchi, S. 1988, ApJ, 330, 695
Ulvestad, J. S. 1982, ApJ, 259, 96
Ulvestad, J. S., Wilson, A. S., & Sramek, R. A. 1981, ApJ, 247, 419
van Gorkom, J. H. 1987, in IAU Symp. 127, Structure and Dynamics of Elliptical Galaxies, ed. T. de Zeeuw (Dordrecht: Reidel), 421
Wannier, P. G. 1980, ARA&A, 18, 399
Wild, W. 1990, Ph.D. thesis, Ludwig-Maximilians-Universität, München, FRG
Wild, W., et al. 1991, ApJ, 368, 622
Willner, S. P., Elvis, M., Fabbiano, G., Lawrence, A., & Ward, M. J. 1985, ApJ, 299, 443
Wilson, A. S., & Willis, A. G. 1980, ApJ, 240, 429
Young, J. S., & Sanders, D. B. 1986, ApJ, 302, 680
Young, J. S., & Scoville, N. 1984, ApJ, 287, 153